Predictive data driven turbulence-combustion model through Super Resolution Generative Adversarial Network

Temistocle Grenga[1], Ludovico Nista[1], Christoph D. K. Schumann[1], Amir N. Karimi[1], Gandolfo Scialabba[1], Mathis Bode[1], Antonio Attili[2], Heinz Pitsch[1]

[1]Institute for Combustion Technology, RWTH Aachen University
[2]School of Engineering, University of Edinburgh

Abstract

The closure of the turbulence problem in reacting flows is challenging since it is strongly affected by heat release. Moreover, the models developed, in general, have been created for non-reacting flows. Innovative machine learning algorithms allow to develop data-driven models able to capture the interaction of turbulence and heat release at different regimes. In this work, the Enhanced Super-Resolution Generative Adversarial Network architecture is proposed as technique to reconstruct the subfilter scales for two planar premixed flames at different Karlovitz number.

Introduction

In Large Eddy Simulation (LES) of turbulent reacting flows the closure of the advection terms and mass source terms in the governing equations is an active area of research, and predictive models remain elusive. For the mass source term in the scalar equation (filtered chemical source term), many classes of models have been developed for both premixed and non-premixed combustion and applied to systems of different complexity with varying degrees of success [1]. The advection terms in the equations for the momentum and the species mass fractions represent unresolved turbulent mixing of the momentum (subfilter stresses) and the scalar (subfilter scalar fluxes).

The models for these terms were, in general, developed for non-reacting flows and then adapted to reacting flows, without any concern for the assumptions in these models. This approach does not accurately account for the effect of heat release on turbulence and precludes the achievement of predictive LES, even with perfect combustion models [2].

Deep neural networks thrive in situations where structural relations between input and output are presumably present but unknown. The reconstruction of subgrid information with deep neural networks is a promising approach to link the large-scale results, obtained from filtered equations, to the actual flow fields. Among various kind of neural networks developed, Super-Resolution Generative Adversarial Networks (SRGANs) have typically been applied to image enhancement, where the input to the generator is a low-resolution image and the model learns to enhance the image and reconstruct it with more details. During training of the SRGAN, the generator learns to generate realistic images, whereas the discriminator becomes more effective at distinguishing the generated images from the real ones. Similarly, in the context of turbulent combustion, SRGANs can be used to generate high-wavenumber detail of lower resolution simulations [3].

The analysis of two turbulent premixed hydrogen/air spatially-evolving planar jet flames at different Karlovitz number (Ka) [4] highlighted the presence of different physical mechanisms driving the heat release-turbulence interaction. In particular, the turbulent kinetic energy budget shows that, below a critical Karlovitz number, the dominant source of kinetic energy is the velocity-pressure gradient correlation linked to the dilatation induced by combustion heat release. While above the critical Karlovitz number, the turbulent kinetic energy budget is similar to a non-reacting flow. The invariant maps of the anisotropic portion of the strain-rate tensor and of the Reynolds stress tensor at high Ka corresponds to pure shear between the central jet and the coflow; for the lower Ka, the dilatation from combustion heat release causes a lengthening of fluid elements.

Data from these DNS calculations are utilized to both train and test a modified SRGAN to then realize a set of predictive data driven models having different characteristics: low-Karlovitz, high-Karlovitz. The models are evaluated with different flames in order to assess their predictive capabilities across different combustion regimes as well as turbulent regimes. This work constitutes the base for the construction of a predictive model for multi-regime turbulent combustion based on a SRGAN enriched with physics-based features.

Database

The Direct Numerical Simulation (DNS) database considered in this work is constituted by two spatially-developing turbulent premixed planar jet flames at Re = 5000 and having different Ka [4]. They are composed of a central jet, which is separated by thin walls from primary coflow jet. Flow in the central jet was initialized from auxiliary DNS calculations of fully-developed turbulent channel flow. Secondary low-velocity bulk coflows isolate the central and coflow jets from the domain boundaries. For these cases, fully-developed laminar velocity profiles are specified at the inlet for the primary coflow jets, and the use of laminar coflows or turbulent coflows was found not to significantly affect the turbulence budgets within the flame.

The central jet consists of a gaseous mixture of hydrogen and oxygen at the stoichiometric equivalence ratio, diluted 80.9% by mass with nitrogen, at $T_0 = 300$ K and $p_0 = 1$ atm. Equilibrium products of combustion of the same mixture issue from the coflow jets at $T_c = 2047.5$ K and $p_c = 1$ atm. A nine species hydrogen chemical

kinetic model [5] is used. The critical Karlovitz number separates two different regimes. For Ka lower than the critical value, (case K1), pressure-dilatation induced by the flame is the primary source of turbulent kinetic energy because it represents the small scales source; conversely, for Ka larger than the critical value, (case K2), mean shear is the dominant source of turbulent kinetic energy.

To generate the DNS database, the Navier-Stokes equations are solved in the low Mach number limit using a semi-implicit iterative algorithm of Desjardins et al. [6], implemented in the code NGA. The species equations are solved with a monolithic scheme using an approximately factorized exact Jacobian.

The domain for case K1 has dimensions 12H0 x 24H0 x 3H0 (with H0 the height of the central jet) in the streamwise (x), cross-stream (y), and spanwise (z) directions, respectively. The computational grid has 768×586×256 points. Case K2 has a longer domain, 24H0 x 16H0 x 3H0, and a finer grid with 1536×576×256 points. The boundary conditions are, in both cases, inflow on the -x face, outflow on +x face, free slip-on y faces, and periodic in the z-direction.

The subdomain considered for the analysis in case K1 has dimensions 7H0×4H0×H0, or rather 390×316×86 grid points, in the x-, y-, and z-directions, respectively. The subdomain contains about 10.6 million grid points, so the number of degrees of freedom per snapshot is about 42 million since four variables (three velocity components, u, v, w, and temperature) are considered. The number of snapshots considered is 401, and the space in time Δt = 4 μs. Subsequently, for this analysis, up to about 17 billion data values are used, or rather more than 300 GB.

In the case of K2, the subdomain considered has dimensions 8H0×4H0×H0, or rather 454×310×86 grid points, containing about 12.1 million grid points. The number of degrees of freedom for each snapshot is about 48 million, and for the complete analysis, 19 billion values are used. The snapshots have been taken with an interval of Δt = 3.25 μs.

Methods

Model description

The network is based on the architecture of Turbulence Super-Resolution Generative Adversarial Network Architecture (TSRGAN) by Bode et. al [7], which itself is based on a 3D Tensorflow [8] implementation of the Enhanced Super-Resolution Generative Adversarial Network Architecture (ESRGAN) [9] originally developed for single image super-resolution tasks. Compared to the original ESRGAN generator, no up-sampling blocks are used, only one residual-in-residual dense block is employed and an additional convolutional layer is added at the end. The TSRGAN generator heavily relies on the use of three-dimensional convolutions layers in combination with leakly rectified linear units (LeaklyReLU) [10] as activation function.

The discriminator architecture differs from the ESRGAN's discriminator by the addition of a dropout layer and a different last but one dense block to account for the additional neurons of the 3D architecture.

Data preparation

To obtain LES-like solutions of the simulations, the datasets were filtered with a truncated Gaussian filter with width Δ = 8dx, resulting in resolved energy levels, defined as

$$\frac{<0.5\,\overline{u_i}\overline{u_i}>}{<0.5\,u_iu_i>},$$

of approximately 86.3% for the flame K1, and 88.2% for the flame K2. There is no downsampling of the domain in this process, and hence the number of points in the DNS and filtered DNS solutions are the same.

Since the entire domain is too large to be used as input to the network due to memory limitations, cropping operations were applied to the domain similar to the patches employed in the single image super-resolution tasks. In order to reduce the likelyhood of the network learning an inverse filtering operation, the cropping size was set to a fixed size of 2Δ in each direction of the cropped boxes, resulting in a box size of 16 grid points. These boxes were randomly selected from subdomains previously described. For each snapshot, 4000 boxes were taken. To artificially increase the dataset size further, random flipping and rotation operations were employed during dataset loading. The boxes were taken at the same location for the filtered DNS data - used as input to the network - and for the DNS data used as label data.

Training strategy

The generator was initially trained independently of the discriminator (pretraining) using the mean squared error (MSE) of the pixel loss.

Later the GAN was trained in a supervised fashion, using a combination of the MSE of the pixel loss, the MSE of the spatial gradient of the pixel loss and the relativistic adversarial loss [11].

The network was trained on three different datasets: K1 data only, K2 data only and a mixture of the two using both datasets completely. Snapshots were selected randomly and eight of them (32000 boxes) were loaded as a dataset at any given time during the training. The generator was trained for 10 epochs on these 8 snapshots, then the next 8 snapshots were loaded and the training process continued for the same number of epochs until there were no more snapshots left. In the same fashion, the GAN was trained afterward. To speed up this training process, the model was trained on the RWTH cluster using 4 NVidia V-100 GPUs on two nodes using the Horovod library [12] for parallelization. The generator was trained with a batch size of 16 whereas the GAN was trained with a mini-batch size of 12.

Two configurations were investigated:

1. Training using only velocity components
2. Training using velocity components, and temperature.

The initial learning rate for the generator was set to 5.0×10^{-5}, with the exception of the case K1 in the configuration with only velocity components where it

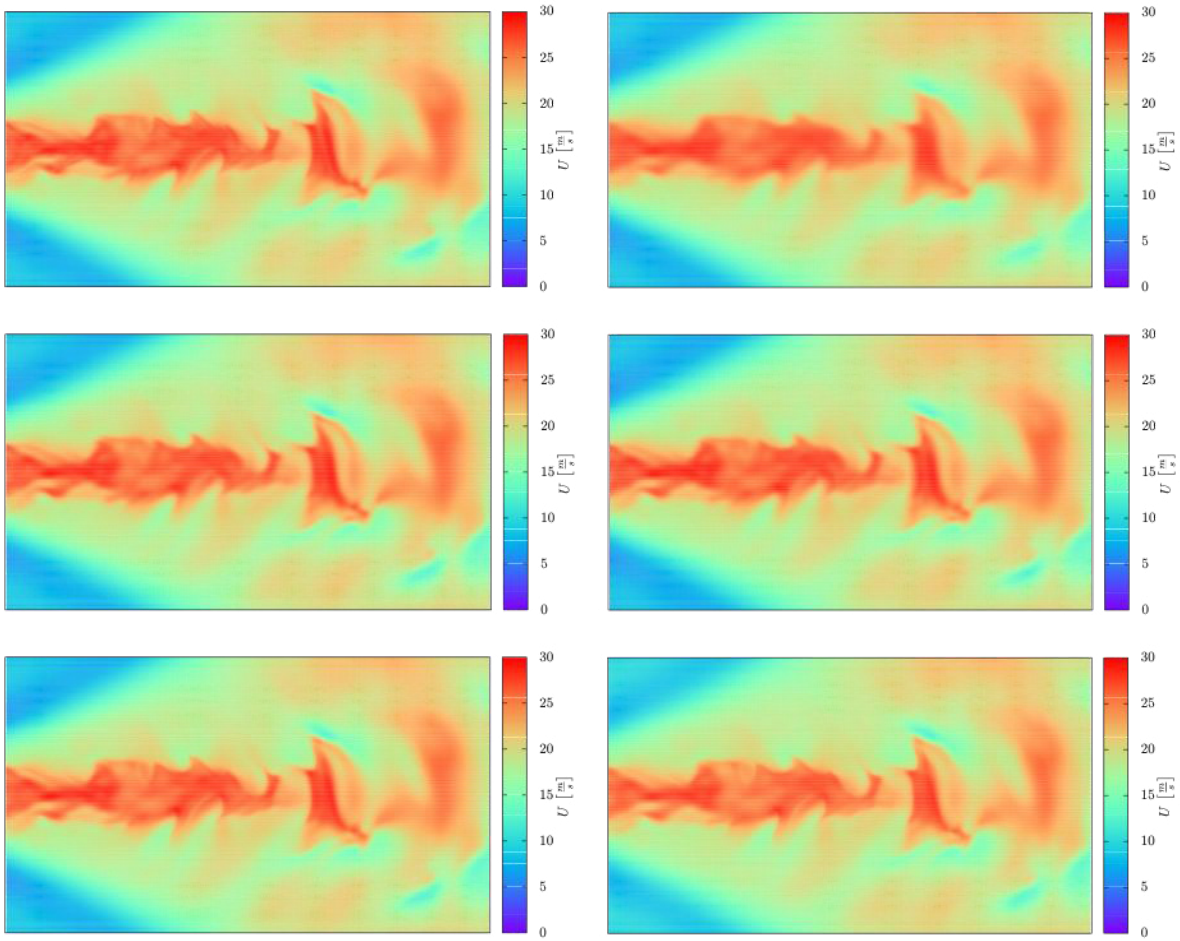

Fig. 1. Velocity fields for K1 case. Top row: DNS (left), filtered-DNS (right); center row: reconstructed fields using model trained with velocity components from K1 data only (left), and a mixture of both datasets (right); bottom row: reconstructed fields using model trained with velocity components and temperature from K1 data (left), and a mixture of both datasets (right).

was set to 3.0×10^{-5}. For both networks of the GAN, instead, the initial learning rate was set to 1.0×10^{-5}. A learning rate scheduler that halves the learning rate every 10k iterations (50k iterations for the first time) is employed. The learning rate was optimized with the Adam optimizer [13].

To normalize the dataset while keeping the relation of the velocity components to another, the maximum and minimum of all velocity components of the entire DNS dataset were used to normalize the velocity components with the same values. Temperature was normalized independently to be between 0 and 1 using their respective minima and maxima from the DNS dataset.

Results and Discussion

In Figure 1 a planar cut of the DNS database of case K1is visualized, along with the corresponding filtered DNS field obtained applying the Gaussian filter as described above. Some turbulence structures are still fairly well clear in the filtered field, however the amount of kinetic energy contained corresponds to the one resolved in a LES. The following panel (center row left) in Figure 1 visualizes the reconstructed field obtained training the TSRGAN with the velocity field of the same case. The RSME of the axial component of the velocity, u, is 0.117m/s, this high accuracy demonstrated the capability of the TSRGAN in learning the flow features at smaller scale. Introducing an additional variable in the training procedure, namely temperature, it seems that more details in the velocity field are reconstructed (bottom row left). Instead, evaluating the RMSE for u yields a slightly higher, 0.191 m/s.

The aim in using both K1 and K2 databases for the training of the TSRGAN is to increase the range of applicability, since it should learn the characteristics of the flows at different flame regimes. The panels on the right side of Figure 1 report the results obtained. These are, in general, less accurate in comparison with the corresponding fields on the left side (RMSE of u equal to 0.166 m/s and 0.535 m/s). However, the loss in accuracy is small in comparison with the possibility to extend the range of TSRGAN.

Figure 2 shows the Joint Probability Density Function (JPDF) for the residual-stresses for the case K1 in the four configurations tested. The panels on the top row confirm that the velocity field is well reconstructed when

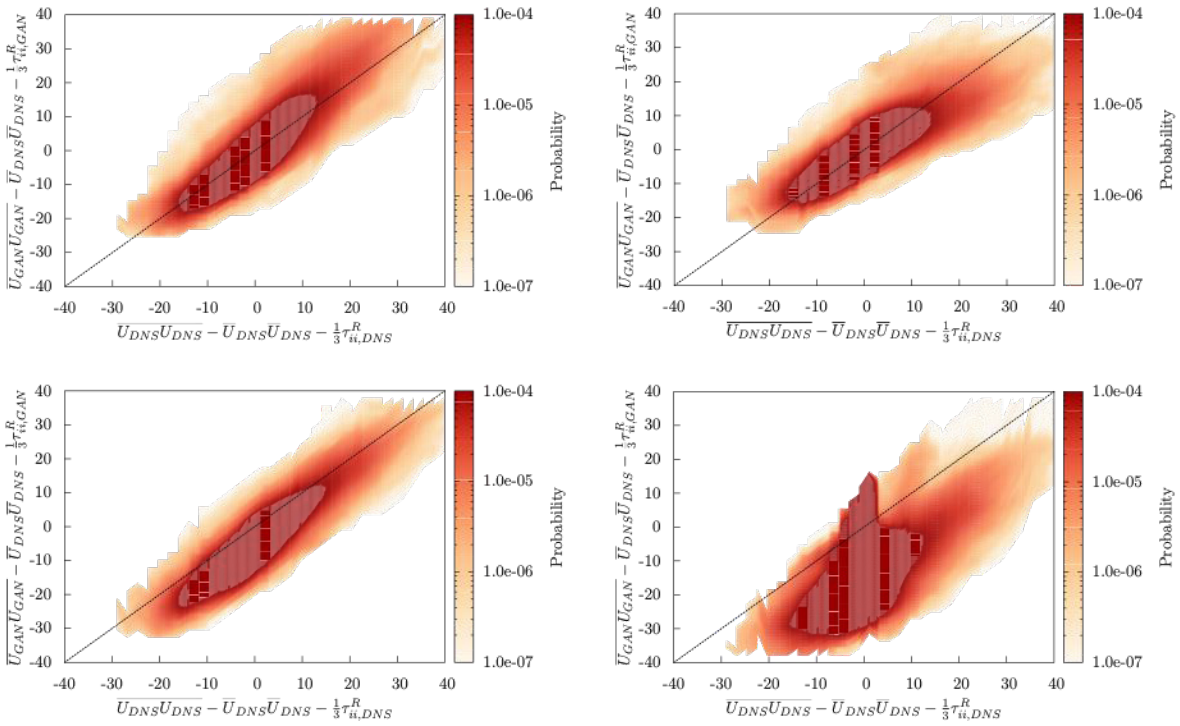

Fig. 2. JPDF of the residual-stress for case K1. Top row: reconstructed fields using model trained with velocity components from K1 data only (left), and a mixture of both datasets (right); bottom row: reconstructed fields using model trained with velocity components, and temperature from K1 data (left), and a mixture of both datasets (right).

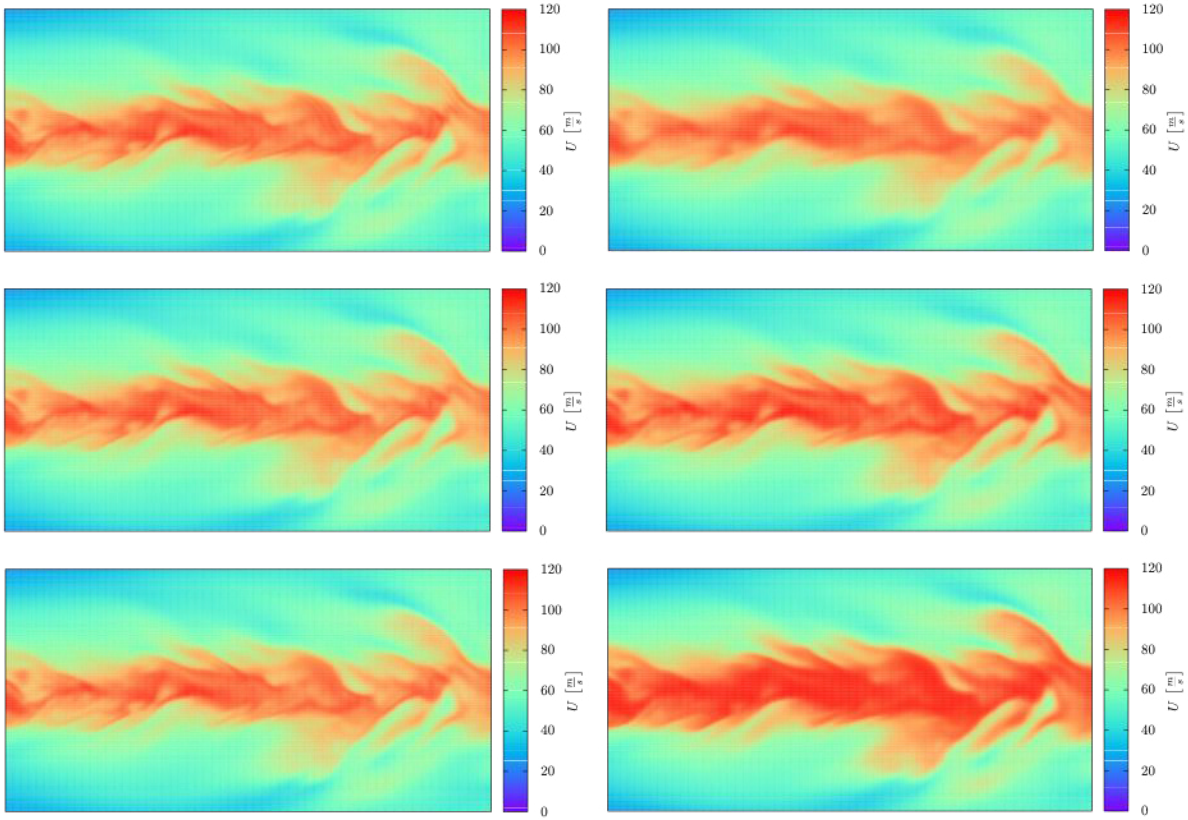

Fig. 3. Velocity fields for K2 case. Top row: DNS (left), filtered-DNS (right); center row: reconstructed fields using model trained with velocity components from K2 data only (left), and a mixture of both datasets (right); bottom row: reconstructed fields using model trained with velocity components, and temperature from K2 data (left), and a mixture of both datasets (right).

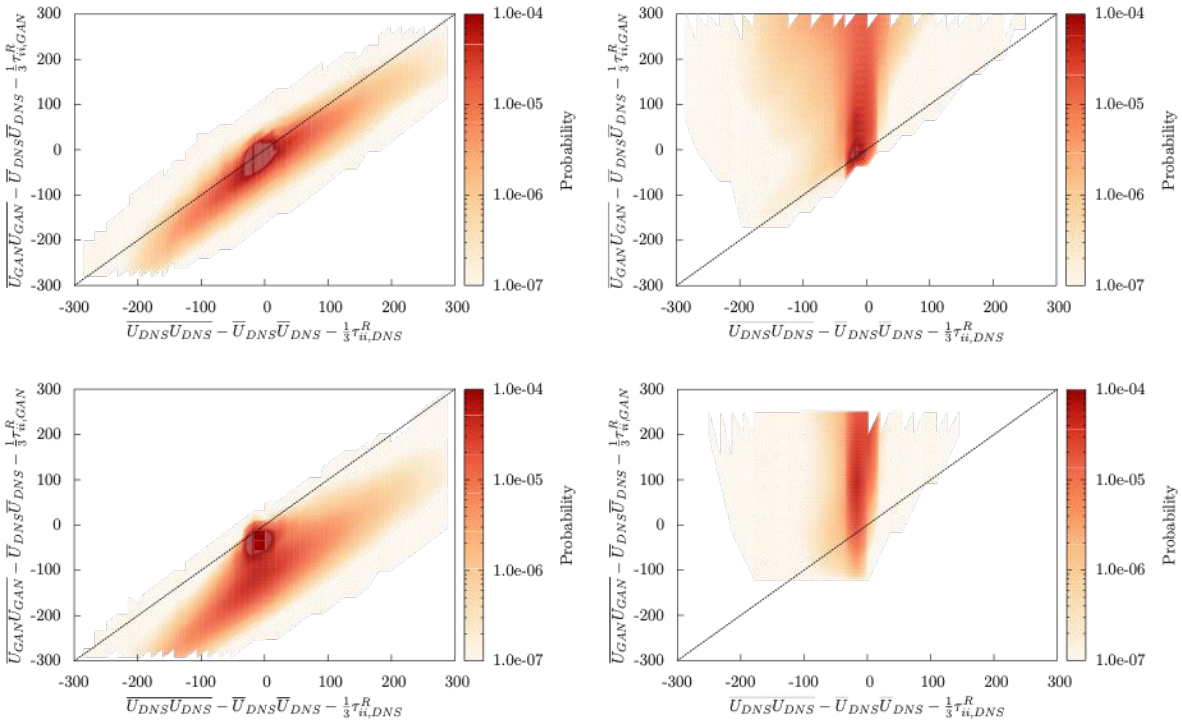

Fig. 4. JPDF of the residual-stress for case K2. Top row: reconstructed fields using model trained with velocity components from K2 data only (left), and a mixture of both datasets (right); bottom row: reconstructed fields using model trained with velocity components, and temperature from K2 data (left), and a mixture of both datasets (right).

only the velocity components are used as input, independently on the databases used. The bottom row of Figure 2 highlights the loss of accuracy obtained adding the temperature as input. On the left side, when only data from K1 are used, there is a small shift to the towards lower values, while this is more marked on the right panel. From these results, it can be stated that the TSRGAN prediction does not improve by adding additional variables, probably because they introduce additional dynamics as well. It has been shown that the heat release and turbulence interaction is driven by different physical mechanisms in the two cases considered [14, 15]. Indeed, in the last plot of Figure 2 the JPDF shows a larger deviation since the TSRGAN attempts to reconstruct different physical phenomena.

Similarly, in Figure 3 and 4 the velocity fields and the JPDF of the residual-stress for the case K2 are reported. Also, in this case the training with the same test case produces more accurate results (RMSE of u 0.342 m/s) compared to the training based on a mixture of the two cases. It is worth to note that in this case adding the temperature in the training has not a large impact on the accuracy because the dynamics are similar to the one for a non-reacting flow. The use of a mixture of the two databases for the training, conversely, introduces a large error visible as high velocity regions in Figure 3, and as high value of the Reynolds stress in Figure 4 since it adds the effect of dilatation due to heat release which is typical of the case K1.

Conclusions

The TSRGAN model has been presented as possible closure model for turbulence for reacting flows at different regimes.

The databases used for training and testing are two planar premixed flames of a hydrogen/air mixture at Re=5000 and at two different Karlovitz number.

The TSRGAN has been proven to be reliable in the reconstruction of the small scales features for each case individually. Some limitation has been found when the TSRGAN is trained with a mixture of the two databases because they contain different physical mechanisms driving the interaction between turbulence and heat release.

Similarly, when additional variables are used to train the network, the accuracy in the prediction of those decreases as they have different correlations and the TSRGAN cannot represent all at the same time.

Further research has to be devoted in order to produce a universal model based on TSRGAN. The characterization of the flows through the non-dimensional quantities, e.g. Re, Ka, has to be integrated in the model.

Acknowledgements

The project was generously supported by the European Research Council (ERC) under the European Union's Horizon 2020 research and innovation program (grant agreement no. 695747)

This work is supported by Computing Time Project on the RWTH Compute Cluster rwth0658.

References

[1] H. Pitsch. Large-eddy simulation of turbulent combustion. Ann. Rev. Fluid Mech., 38:453–482, 2006.

[2] N. Peters. Laminar diffusion flamelet models in non-premixed turbulent combustion. Prog. Energy Combust. Sci., 10:319–339, 1984.

[3] M. Bode, M. Gauding, Z. Lian, D. Denker, M. Davidovic, K. Kleinheinz, J. Jitsev, and H. Pitsch. Using physics-informed enhanced super-resolution generative adversarial networks for subfilter modeling in turbulent reactive flows. Proceedings of the Combustion Institute, 2021. https://doi.org/10.1016/j.proci.2020.06.022.

[4] J. F. MacArt, T. Grenga, and M. E. Mueller. Effects of combustion heat release on velocity and scalar statistics in turbulent premixed jet flames at low and high karlovitz numbers. Combustion and Flame, 191:468 – 485, 2018.

[5] S.G. Davis, A.V. Joshi, H. Wang, F. Egolfopoulos. An optimized kinetic model of H2/CO combustion. Proc. Combust. Inst., 2005, 30(1), 1283-1292.

[6] O. Desjardins, G. Blanquart, G. Balarac and H.Pitsch, High order conservative finite difference scheme for variable density low Mach number turbulent flows. J. Comput. Phys., vol. 227, p. 7125–7159, 2008.

[7] M. Bode, M. Gauding, Z. Lian, D. Denker, M. Davidovic, K. Kleinheinz, J. Jitsev, and H. Pitsch. Using physics-informed super-resolution generative ad- versarial networks for subgrid modeling in turbulent reactive flows. arXiv, 2019.

[8] M. Abadi, P. Barham, J. Chen, Z. Chen, A. Davis, J. Dean, M. Devin, S. Ghemawat, G. Irving, M. Isard, et al., "Tensorflow: A system for large-scale machine learning," in 12th {USENIX} symposium on operating systems design and implementation ({OSDI}16), 2016, pp. 265–283.

[9] X. Wang, K. Yu, S. Wu, J. Gu, Y. Liu, C. Dong, C. C. Loy, Y. Qiao, and X. Tang. Esrgan: Enhanced super- resolution generative adversarial networks. Computer Vision – ECCV 2018 Workshops. ECCV 2018.

[10] A. Géron, Hands-on machine learning withScikit-Learn, Keras, and TensorFlow: Concepts,tools, and techniques to build intelligent systems. O'Reilly Media, 2019

[11] A. Jolicoeur-Martineau. The relativistic discriminator: a key element missing from standard gan. arXiv, 2018.

[12] A. Sergeev and M. Del Balso. Horovod: fast and easy distributed deep learning in tensorflow. arXiv, 2018.

[13] D. P. Kingma and J. L. Ba. Adam: A method for stochastic optimization. 3rd International Conference for Learning Representations, 2014.

[14] J. F. MacArt, T. Grenga, and M. E. Mueller. Evolution of flame-conditioned velocity statistics in turbulent premixed jet flames at low and high Karlovitz numbers. Proc. Combust. Inst., 37:2503 – 2510, 2019.

[15] T. Grenga and M. E. Mueller. Dynamic Mode Decomposition: A Tool to Extract Structures Hidden in Massive Datasets. In Data Analysis for Direct Numerical Simulations of Turbulent Combustion, Springer, 2020.